Flow Measurement and Instrumentation 64 (2018) 14–27

Contents lists available at ScienceDirect

Flow Measurement and Instrumentation

journal homepage: www.elsevier.com/locate/flowmeasinst

Transverse velocity profiling under positive surges in channels

Xinqian Leng, Hubert Chanson*

The University of Queensland, School of Civil Engineering, Brisbane, QLD 4072, Australia

ARTICLE INFO

Keywords:
Positive surges
Transverse velocity profiling
Instantaneous velocity
Transient open channel flows
Compression waves
Integral turbulent time and length scales

ABSTRACT

A positive surge is a sudden rise in water surface elevation in an open channel flow. It is an unsteady rapidly-varied flow which may propagate over long distances. Herein new transverse velocity profiling experiments were conducted in steady and unsteady rapidly-varied flows. The measurements were performed with a transverse ADV Profiler and an array of two ADV Profilers, installed perpendicular to each other. The results were systematically compared to ADV Vectrino+ data. Ensemble-averaged velocity measurements demonstrated that the transverse Profiler gave satisfactory performances in a highly unsteady positive surge flow. The ensemble-averaged velocity and Reynolds stress characteristics measured by the transverse Profiler, alone or in an array, were similar to results with a traditional ADV and the vertical Profiler alone, although it is acknowledged that the ADV Vectrino II Profiler instrument has intrinsic limitations. The one-dimensional integral turbulent time and length scales were comparable in magnitudes in the transverse or vertical directions, with the turbulent length scale ranging from 10^{-3} m to 10^{-2} m and turbulent time scales from 10^{-2} s and 10^{-1} s, depending upon the flow phase. The turbulent length and time scales tended to increase during and after the surge passage, in comparison to those during the initially steady flows.

1. Introduction

A positive surge is a sudden rise in water surface elevation in an open channel flow [13]. It may be generated by an increase in discharge induced by an upstream control structure, or a reduction in flow rate following the closure of a downstream gate. The surge may propagate over long distances and is associated with intense unsteady turbulence mixing [14,19]. Engineering applications encompass rejection surges and load acceptance surges in hydropower canals [26,7]. Geophysical applications cover tidal bores in estuaries, up-river tsunami bores, and landslide-generated water waves [11,23,28,4].

Leng and Chanson [20] first showed the application of a fast response profiling system, the Nortek™ acoustic Doppler velocimeter (ADV) Vectrino II Profiler, to characterise the unsteady turbulence generated by positive surges. Introduced in 2010, the Vectrino II Profiler, i.e. ADV Profiler, is a high-resolution acoustic Doppler velocimeter developed to measure turbulence, based upon coherent Doppler processing [25,30,31]. In steady flows, several studies documented a number of validation issues and measurements errors [20,30,6,8]. In unsteady open channel flows, however, Leng and Chanson [20] showed that "*the performance of ADV Vectrino II Profiler […] was satisfactory provided that a careful validation was undertaken*". To date all studies were conducted with a downward-looking head, hence a vertical velocity profile. Horizontal velocity profiling has been rarely undertaken in open channel flows. Limited steady flow applications include acoustic tomography [1] and horizontal current profiling H-ADCP [12,16], yielding typically time series of instantaneous discharge observations.

In positive surges, three-dimensional flow structures were reported in both physical observations [18,32] and CFD modelling [17,27]. In the present study, new horizontal velocity profiling measurements were performed under carefully controlled flow conditions to characterise turbulence induced by three-dimensional vortical structures. Both steady and unsteady measurements were conducted in a large laboratory flume. Experiments were also performed with an array of two ADV Profilers, mounted transversely and vertically. An ensemble-averaged technique was applied to unsteady flows to investigate positive surges. The quality and accuracy of the Profiler and Profile array data sets were systematically validated against data collected with a traditional acoustic Doppler velocimeter.

2. Experimental facility and instrumentation

2.1. Physical facility

Experiments were conducted in a 19 m long 0.7 m wide rectangular

* Corresponding author.
E-mail address: h.chanson@uq.edu.au (H. Chanson).

https://doi.org/10.1016/j.flowmeasinst.2018.10.006
Received 4 March 2018; Received in revised form 19 July 2018; Accepted 7 October 2018
Available online 11 October 2018
0955-5986/

test section, equipped with a smooth PVC bed and glass sidewalls, previously used by Leng and Chanson [19,20]. The bed slope was horizontal herein. The water discharge was delivered through an upstream tank equipped with baffles and flow straighteners, followed by a smooth three-dimensional convergent, ending at the start of the test section. The flow rate was measured with a magneto flow meter, previously calibrated on site. The positive surge was generated by the rapid closure of a downstream Tainter gate placed at x = 18.1 m, where x is the longitudinal distance measured from the test section's upstream end. The time of gate closure was less than 0.2 s and did not affect the characteristics of the surge nor the unsteady velocity field.

The water depth was measured with pointer gauges in steady flow with an accuracy of 0.001 m. In unsteady flow, the water depth was recorded non-intrusively using acoustic displacement meters Microsonic™ Mic+ 25/IU/TC and Mic+ 35/IU/TC installed along and above the water surface. All the displacement meters were calibrated against the pointer gauges in steady flow and were sampled at 100 Hz in unsteady flows.

2.2. Velocity measurements

Three velocimeter units were considered in the present study: a Nortek™ ADV Vectrino+ (Hardware ID VNO 0436), a Nortek™ ADV Vectrino II Profiler equipped with a downlooking head and fixed stem (Serial number P27338, Hardware ID VNO 1366), and a Nortek™ ADV Vectrino II Profiler equipped with a flexible head and mounted sidelooking (Hardware ID VNO 1436, firmware ID 1950). The two ADV Vectrino II Profilers herein were not re-calibrated, following the 2016 worldwide recall of ADV Vectrino II by the manufacturer. Fig. 1 presents photographs of the transverse Profiler unit.

The transverse Profiler was mounted at x = 8.425 m. When in use, the vertical Profiler was installed at x = 8.5 m. Fig. 2 presents the sampling profile of the Profilers. Both Profilers were configured to quasi-simultaneously sample the velocity at 100 Hz for 35 sampling points in a 35 mm profile. The velocity range was ± 1.0 m/s or ± 1.5 m/s. The Profilers were synchronised to sample simultaneously with the acoustic displacement meters. The synchronisation between instruments was within ± 1 ms.

Steady flow Profiler data were post-processed by the MATLAB program VTMT version 1.1, designed and written by Jan Becker [2]. The post-processing included the removal of data with average correlation values less than 60% and average signal to noise ratio less than 5 dB, and spurious data point removal using the phase-space thresholding technique. In unsteady flows, such a post-processing technique was not applicable (Nikora 2004, *Person. Comm.*, [3,15]) and raw data were used directly for analysis, following Leng and Chanson [20].

2.3. Experimental programme

Steady and unsteady flow experiments were conducted using either a single ADV Vectrino+ , the tranverse Profiler (Figs. 1 and 2a), the vertical Profiler, or an array of both transverse and vertical Profilers (Figs. 2b & 3). In unsteady flows, the experiments were repeated 25 times and the results were ensemble-averaged, following Chanson and Docherty [5] and Leng and Chanson [19,20]. For the Profiler array measurements, a small longitudinal separation (Δx = 75 mm) between the sampling profiles was set to prevent adverse interactions between the two instruments. Such interactions were studied in steady and unsteady flows [21]. The Profiler array setup was designed based upon the results of these preliminary investigations.

Steady flow experiments were conducted for Q = 0.10 m^3/s and a horizontal channel bed slope. Positive surge experiments were performed for an initial discharge Q = 0.10 m^3/s, a horizontal bed slope, and a positive surge Froude number Fr_1 = 1.55, corresponding to a breaking surge (Figs. 1c & 3). The positive surge was generated by the fast closure of the downstream Tainter gate, and each run sampling was

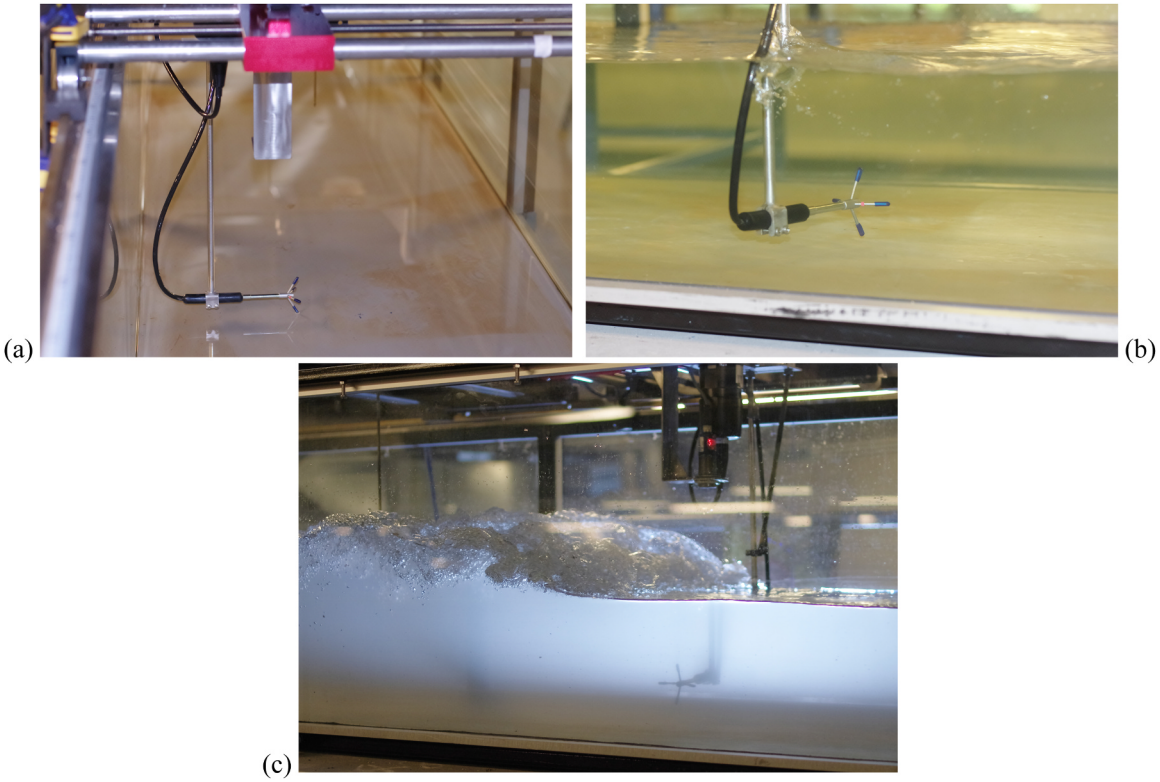

Fig. 1. Experimental settings of transverse ADV profiling: (a) ADV Profiler in dry flume; (b) Sideview of ADV Profiler in a steady flow (Q = 0.1 m^3/s, flow direction from left to right); (c) ADV Profiler during positive surge passage for Q = 0.1 m^3/s and Fr_1 = 1.55, surge propagation from left to right.

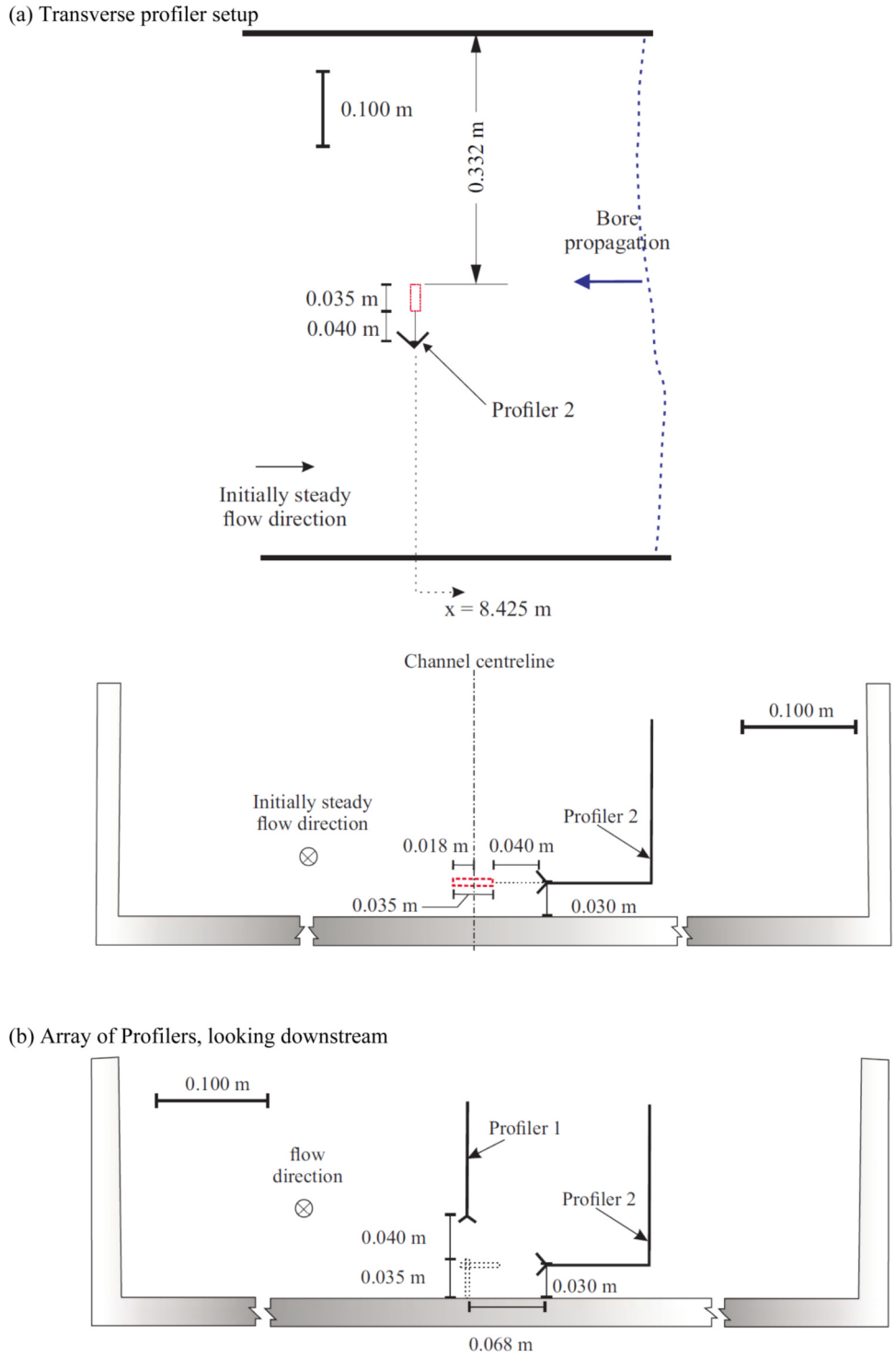

Fig. 2. Dimensioned sketches of Profiler setups. (a) Transverse profiler setup. (b) Array of Profilers, looking downstream.

stopped when the surge reached the upstream end of the test section. Fig. 3 presents a sequence of four photographs of the positive surge advancing past the Profiler array.

3. Steady flow measurements using a transverse Profiler

Steady flow measurements were repeated at x = 8.5 m with the ADV Vectrino+ and the transverse Profiler. Sampling was conducted for 60 s at 200 Hz for the ADV and for 90 s at 100 Hz for the Profiler. The ADV data were recorded on the channel centreline (y/B = 0.5). Horizontal velocity profiles were undertaken for $0.17 < z/d < 0.86$ and $0.22 < y/B < 1.00$, where z is the vertical elevation of the sampling profile, y is transverse distance from the right sidewall, d is the water depth and B is the channel width. Note that all receivers of the Profiler were always under water during the experiments. Fig. 4a shows typical transverse profiles of the longitudinal velocity and velocity fluctuations measured by the transverse Profiler, with comparison to the ADV data.

For all vertical elevations, the side-looking mounted Profiler showed some good estimation of the time-averaged velocity for the majority of

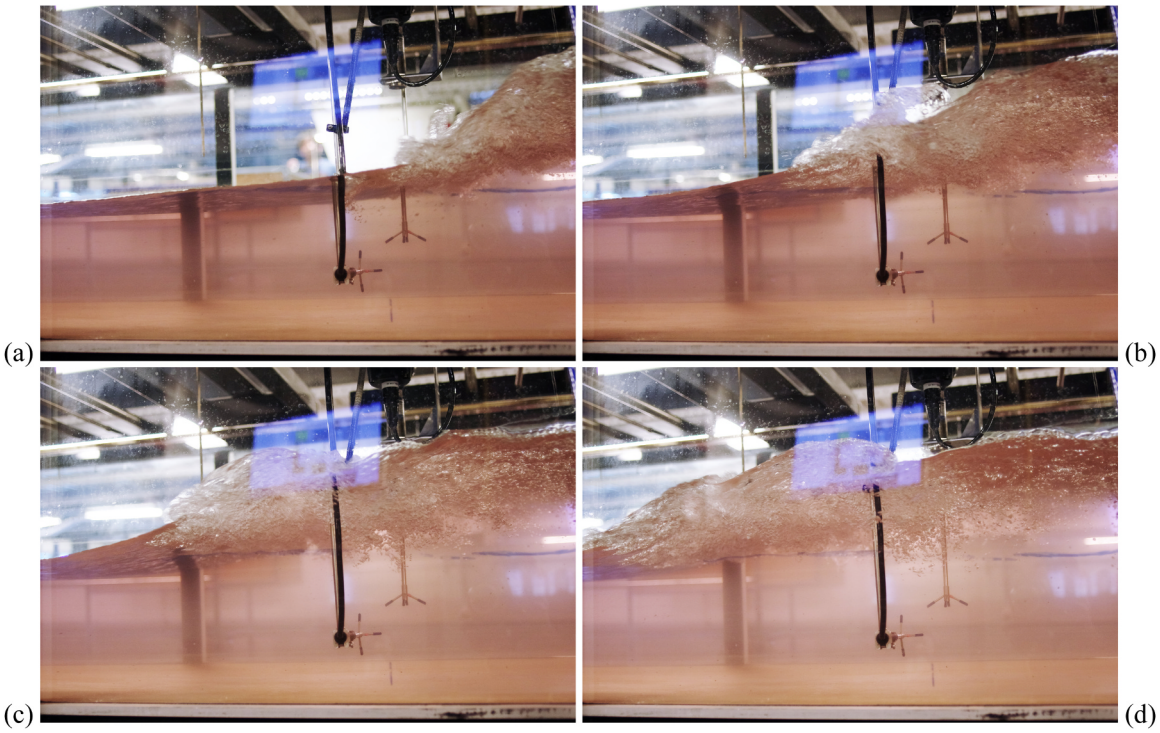

Fig. 3. Positive surge propagation past the array of vertical and transverse ADV Profilers for Q = 0.1 m^3/s and Fr_1 = 1.55, surge propagation from right to left (a) t = t_o; (b) t = t_o + 0.12 s; (c) t = t_o + 0.24 s; (d) t = t_o + 0.36 s.

sampling points in a transverse profile (Fig. 4a). The velocity magnitudes agreed well with centreline ADV data at comparable vertical elevations. A few outliers were observed, as marked in Fig. 4a. Similar errors were previously documented by Zedel and Hay [31], Macvicar et al. [22], and Leng and Chanson [20], often next to the profile edges. The number and proportion of outliers were small, usually less than 5 points in a 35-point sampling profile: they could be easily identified and removed during data analysis. Previous studies also highlighted inaccurate estimation of root-mean-square (RMS) of Profiler velocity data [20,31,8]. The present study found spurious shapes and values, in terms of the horizontal profile of velocity RMS, especially for the longitudinal component. The longitudinal velocity RMS v_x' showed a curved profile across the transverse sampling range (Fig. 4a). Only a small portion of this profile was associated with meaningful values of standard deviations (y/B = 0.48–0.50), close to centreline ADV data at similar vertical elevations. A few outliers were highlighted between y/B = 0.484 and 0.490 (approximately 5 outlying points). The transverse and vertical velocity components tended to show a better agreement with the ADV data, both in terms of time-averaged velocity and velocity fluctuations.

Using the transverse Profiler, a developing boundary layer was documented close to the channel sidewall between y/B = 0.95–1.00 (Fig. 4b). At different vertical elevations, the boundary layer showed different characteristics. At the lowest elevation, the boundary layer appeared to be associated with smaller thickness and lower free-stream velocity, as it interacted with the bottom boundary layer. The three highest vertical elevations were associated with a comparable boundary layer thickness (Fig., 4b).

About the channel centreline, transverse profiles were performed at several vertical elevations for 0.17 < z/d_1 < 0.86. The results highlighted a number of features. Firstly, the transverse Profiler seemed to estimate the transverse and vertical velocity components with a better accuracy, than the longitudinal velocity component. The longitudinal velocity was best estimated at a certain transverse range encompassing the channel centreline (y/B = 0.490–0.515), and poorly at y/B = 0.485 – 0.49 and 0.515 – 0.525. The performances of the Profiler were consistent throughout the water column. That is, for a fixed transverse range, the shapes of the velocity profiles were self-similar at different vertical elevations. With increasing vertical elevations, the data quality in terms of longitudinal velocity fluctuation decreased, with consistent increase of standard deviation at the right end of the profile. The same trend was observed for the transverse velocity component. At lower vertical elevations, the data showed good agreement to the ADV results. The vertical velocity component was associated with better estimations in velocity fluctuations, with a comparatively flat transverse profile throughout the vertical range.

Overall, the present results showed that the transverse Profiler gave satisfactory time-averaged velocity data in the longitudinal, transverse and vertical directions. The velocity fluctuations, characterised by the RMS of the velocity data, were not estimated as well. Within a transverse profile, there were a number of points where the time-averaged velocity was poorly estimated. These points, called error points or weak spots, could range from a small proportion of the profile (5 out of 35 sampling points) to nearly half of the profile points. The number and location of these error points may change when the position of measurement changed, transversely or vertically. However, for a fixed location, the presence of the error points was consistent. Thus a test location must be experimented first to know the error points in a profile and exclude them in subsequent analysis and discussion. With the transverse Profiler, the transverse velocity profile could be sampled, although in an intrusive way. In order to hold the flexible-head, a steel rod has to be intruded into the water, with a grabber to hold the probe head (Fig. 1). The radius of the probe and the radius of the grabber were both non-negligible, creating a wake region downstream of the probe. The wake region did not seem to affect the velocity output of the Profiler, based upon the present results.

4. Unsteady velocity measurements using a transverse Profiler

The propagation of the positive surge induced a rapidly-varied unsteady turbulent flow motion (Fig. 3). The water depth was associated

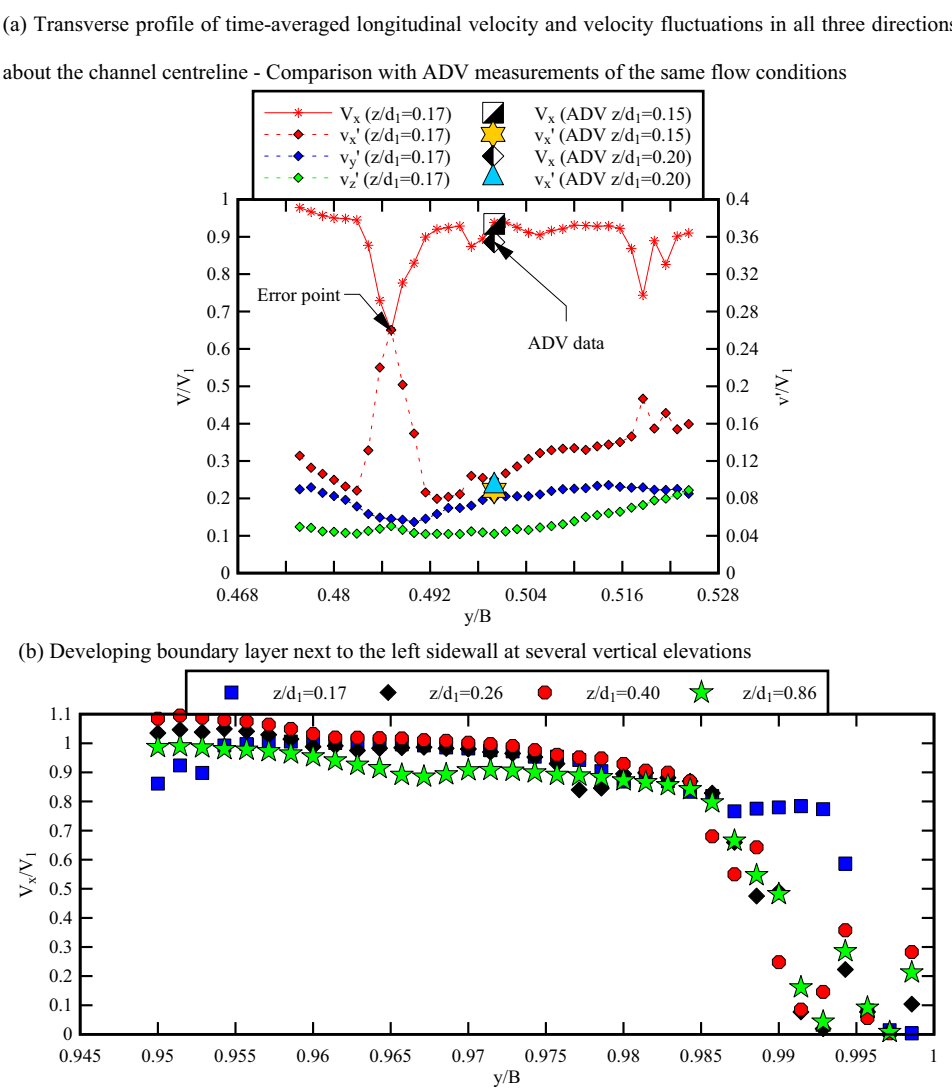

Fig. 4. Distributions of velocity components in steady flows - Q = 0.10 m^3/s, horizontal slope, x = 8.5 m, d = 0.174 m. (a) Transverse profile of time-averaged longitudinal velocity and velocity fluctuations in all three directions about the channel centreline - Comparison with ADV measurements of the same flow conditions. (b) Developing boundary layer next to the left sidewall at several vertical elevations.

with an abrupt rise when the surge front arrived. The velocity data showed characteristic features. The longitudinal velocity decreased rapidly as the free-surface increased (Fig. 5). Negative longitudinal velocity was reached at the end of the deceleration phase, indicating a transient flow recirculation. This transient recirculation velocity was observed at all transverse locations for low vertical elevations ($z/d_1 < 0.3 – 0.5$), with different timings at different transverse locations. Herein d_1 and V_1 are respectively the initial water depth and mean velocity at the sampling location, g is the gravity acceleration and t is the time since Tainter gate closure. Fig. 5 presents ensemble-averaged data, in which the velocity fluctuations are characterised in terms of the difference between the 3rd and 1st quartiles (V_{75}-V_{25}). For a data set with Gaussian distribution, (V_{75}-V_{25}) should be equal to 1.3 times the standard deviation of the data set (Spiegel 1972). For completeness, the ADV data were sampled at 200 Hz on the channel centreline.

Overall, at all vertical elevations on the channel centreline, the results showed a close agreement between all three instrumentations (Fig. 5). Fig. 5 shows a typical comparison between ADV, vertical Profiler and transverse Profiler in terms of the ensemble averaged longitudinal velocity and velocity fluctuations. Note that the ADV data were recorded at a slightly lower vertical elevation $z/d_1 = 0.10$ compared to 0.17 for the Profiler data sets, and hence had a lower median velocity. Rapid decelerations were observed when the surge passed, and transient recirculation velocity was noted at the end of the deceleration phase for all three data sets. The two Profiler data were very close, both quantitatively and qualitatively, during the initially steady flow phase and the rapid deceleration phase. After the deceleration phase, differences were seen between the two Profiler data sets. Namely, the transverse Profiler data set was associated with a longer period of recirculating flow, marked by negative longitudinal velocity.

The velocity fluctuations were of the same magnitudes and similar time-variations were observed throughout the steady flow and bore propagation, for all three data sets. The velocity fluctuations tended to reach maximum values shortly after the bore arrival. The present results showed some difference between ADV and Profiler data. Only some velocity component at certain transverse locations were associated with marked peaks in velocity fluctuations associated with the arrival of the bore. Other velocity components at other locations either showed some increase with no obvious peak during the longitudinal deceleration phase, or no marked difference at all. After the surge passage and longitudinal deceleration phase, all velocity components were associated with smaller fluctuations compared to the initially steady flow, except for the transverse velocity at some vertical elevation.

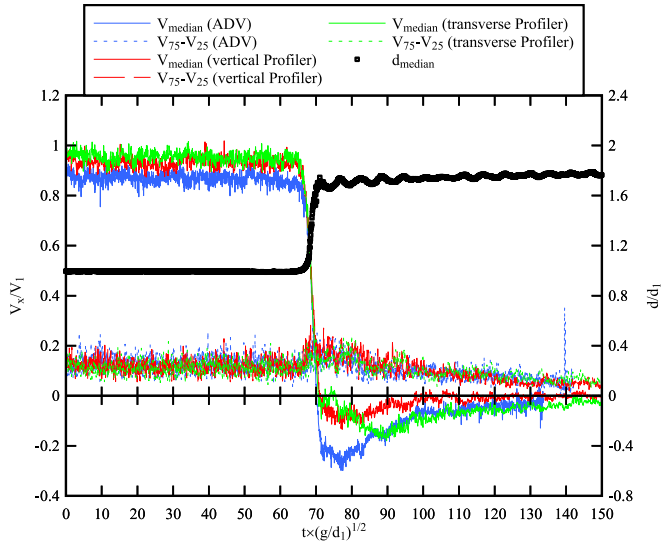

Fig. 5. Comparison between ensemble-averaged water depth and velocity measurements using ADV, vertical Profiler and transverse Profiler during positive surge passage - All measurements conducted on channel centreline y/B = 0.50, z/d_1 = 0.10 (ADV) and 0.17 (vertical & transverse Profilers).

5. Unsteady velocity measurements using an array of Profilers

In the previous section, a single Profiler was used. Herein, experiments with the array of two Profilers were conducted about the channel centreline (0.46 < y/B < 0.51) at three vertical positions: z/d_1 = 0.17, 0.26 and 0.40. The configuration setup is shown in Fig. 2b. A key feature was the simultaneous sampling of the two Profilers, allowing to assess the interferences between the instruments.

In the initially steady flow, the longitudinal velocity measured by transverse Profiler differed significantly from that measured simultaneously by vertical Profiler, i.e. by almost 20%. Such a difference was considered large and could be caused by interactions between the two Profilers.

The ensemble-averaged longitudinal velocity measured by both Profilers showed almost simultaneous deceleration associated with the rapid increase in water depth, marking the arrival of a surge. With the arrival of a positive surge, a transient recirculation was often observed at low vertical elevations, marked by the negative transient longitudinal velocity at the end of the deceleration phase. Both Profilers recorded some transient longitudinal recirculation velocity at elevations up to z/d_1 = 0.42. For comparison, ADV data showed transient recirculation up to an elevation of z/d_1 = 0.50.

The longitudinal velocity fluctuations were associated with some sharp increase, recorded by both Profilers, as the bore passed, except at the end points of a sampling profile (z/d_1 = 0.03 and y/B = 0.50, highlighted by yellow dotted lines). Past experiments documented issues with the Profilers in estimating the velocity variance at the end points of a Vectrino II sampling profile [22,31,6,8]. At the other locations, the longitudinal velocity fluctuations reached a maxima shortly after the arrival of the surge. This maximum velocity fluctuation and its time lag relative to the bore arrival were previously observed in positive surges [19]. The velocity fluctuations in the longitudinal direction showed very comparable results for the two Profilers, both qualitatively and quantitatively.

The ensemble-averaged transverse velocity data, measured by both Profilers, fluctuated drastically as the tidal bore passed. The transverse velocity data showed an abrupt increase and then decrease shortly after the arrival of the surge. Very large oscillations in transverse velocity

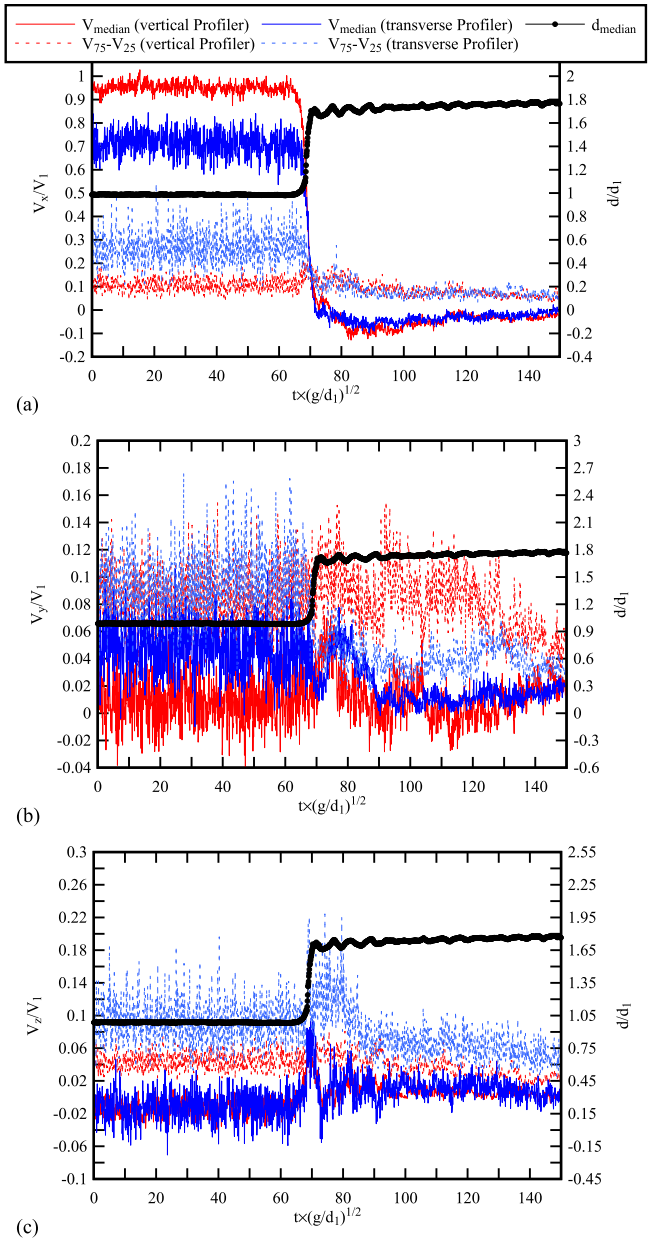

Fig. 6. Ensemble-averaged time-variations of the longitudinal (a), transverse (b) and vertical (c) velocity components measured by the Profiler array at z/d_1 = 0.17, y/B = 0.50 - Same legend for all graphs.

fluctuations were recorded at the later stage of flow after the bore passage, with amplitudes twice as large as the velocity magnitudes. The pattern could be associated with some transverse recirculation eddy and mixing cell, linked to some large-scale vortical structures. The vertical velocity components showed a rapid acceleration then deceleration associated with the bore arrival, as measured by both Profilers. Both Profilers recorded vertical velocity fluctuations twice the magnitudes of the ensemble-averaged vertical velocity component. Peak fluctuations were reached shortly after the surge passage.

The ensemble-averaged velocity characteristics measured by the two Profilers were compared at almost the same location; i.e., same z/d_1 = 0.17 and y/B = 0.50, with a difference in x direction Δx = 0.075 m. Fig. 6 shows a set of typical results. The steady longitudinal velocity before the bore arrival measured by the two Profilers differed,

with smaller transverse Profiler data by almost 20%. This could be caused by the interactions between the two Profilers. During the rapidly-varied flow phase, associated with the bore passage, the two Profilers showed nearly identical results, with the same deceleration gradient and reaching almost the same values of recirculation velocity at the end of the deceleration phase. After the bore passage, the ensemble-averaged longitudinal velocity components measured by the two Profilers were very similar, with almost no difference in terms of the magnitudes and variations with time.

Although the two Profilers were separated by $\Delta x = 0.075$ m, no discernible time lag was observed in terms of the timing of the longitudinal velocity deceleration, and of the acceleration of the vertical velocity. However, some time lag was observed in terms of the transverse velocity component (Fig. 6b). The ensemble-median transverse velocity showed some large fluctuation following the arrival of the bore. A peak in transverse velocity was noted for both Profiler measurements. The two peaks of the two instruments had a dimensionless time difference $\Delta t \times (g/d_1)^{1/2} = 2.7$, corresponding to a time difference of 0.36 s. With a local bore celerity of 1.14 m/s, this would yield a length scale of 0.41 m, which was significantly larger than the physical distance $\Delta x = 0.075$ m between the two instruments. This time lag was not caused by the difference in bore arrival times at the two instruments, but by the transverse motion of the bore itself. This could be confirmed by the ensemble-averaged vertical velocity data of the two Profilers. Both Profilers recorded an abrupt acceleration and deceleration of the vertical velocity with the bore passage. The results of the two Profilers almost overlapped during the acceleration then deceleration phase, highlighting a maximum vertical velocity nearly at the same time. The results demonstrated that the propagation of a tidal bore was a three-dimensional process, with turbulent properties rapidly-varied in all three directions.

The velocity fluctuations showed general trends with some marked increase linked to the bore arrival in all directions, measured by the two Profilers. The transverse Profiler data were generally associated with larger velocity fluctuations in all directions compared to vertical Profiler measurements. Some data were associated with peaks in velocity fluctuations, and were more commonly observed in the transverse and vertical components.

6. One-dimensional turbulent time and length scales

6.1. Presentation

The turbulent integral length and time scales represent respectively the length scale of a characteristic eddy and its lifespan in turbulent flows [10,9]. By cross-correlating the instantaneous velocity signals between two points at (y_1, z) and (y_2, z) along a transverse profile, the cross-correlation function for the i-th velocity component in the transverse direction is:

$$R_{y1y2,i}(\tau) = \frac{\overline{v_{y1,i}(t) \times v_{y2,i}(t+\tau)}}{\sqrt{\overline{v_{y1,i}}^2 \times \overline{v_{y2,i}}^2}} \quad (1)$$

where i = x, y, or z, and the instantaneous turbulent velocity fluctuation v is the deviation of the measured velocity from the ensemble-median velocity: $v = V - \bar{V}$, with V is the measured instantaneous velocity component and $\bar{V}$ the ensemble-median velocity following Chanson and Docherty [5].

Similarly, the cross-correlation function for the i-th velocity component along a vertical profile is:

$$R_{z1z2,i}(\tau) = \frac{\overline{v_{z1,i}(t) \times v_{z2,i}(t+\tau)}}{\sqrt{\overline{v_{z1,i}}^2 \times \overline{v_{z2,i}}^2}} \quad (2)$$

The turbulent length scale can thus be calculated in the transverse and vertical directions for the i-th velocity component:

$$L_{yy,i} = \int_0^{\Delta y_{max}} (R_{y1y2,i})_{max} \times dy \quad (3)$$

$$L_{zz,i} = \int_0^{\Delta z_{max}} (R_{z1z2,i})_{max} \times dz \quad (4)$$

where $(R_{y1y2,i})_{max}$ and $(R_{z1z2,i})_{max}$ are the peaks of the cross-correlation functions between the two points (y_1, z) and (y_2, z), and (y, z_1) and (y, z_2) respectively, and Δy_{max} and Δz_{max} are the maximum separations between two points in the two directions. Herein, Δy_{max} and Δz_{max} equal 34 mm.

The turbulent integral time scale in the transverse and vertical directions for the i-th velocity component is defined as:

$$T_{yy,i} = \frac{1}{L_{y,i}} \times \int_0^{\Delta y_{max}} (R_{y1y2,i})_{max} \times T_{y1y2,i} \times dy \quad (5)$$

$$T_{zz,i} = \frac{1}{L_{z,i}} \times \int_0^{\Delta z_{max}} (R_{z1z2,i})_{max} \times T_{z1z2,i} \times dz \quad (6)$$

where $T_{y1y2,i}$ and $T_{z1z2,i}$ are the integrals of the cross-correlation functions between the time lag associated with peak correlation and the first intersection of the function with zero in the z and y directions [10].

During the initially steady flow phase before the positive surge arrival, cross-correlation calculations were performed for velocity data over 60 s starting from the beginning of the experiment. During the rapidly-varied deceleration flow phase (RVF), the calculations were performed only for data during the rapid deceleration (1–3 s). The calculation of the early flood tide phase was performed for 10 s of data, starting from the end of the RVF phase.

6.2. Transverse cross-correlation measurements

At all transverse separations Δy, the cross-correlation functions $R_{yy,x}$, $R_{yy,y}$ and $R_{yy,z}$ demonstrated quasi-symmetrical bell shapes, with marked maxima or minima along the axis of symmetry. The maximum amplitude of the cross-correlation coefficient R_{max}, could be positive or negative depending on the transverse separation, and occurred with a time lag. This time lag, called optimum time lag T_i, varied with the transverse separation Δy. The maximum cross-correlation coefficient R_{max} also varied with time lag and space. Typical cross-correlation functions $R_{yy,x}$ are presented in Fig. 7, for the longitudinal velocity component at different phases of the positive surge. Typical relationships between R_{max}, T_i and the transverse separation distance Δy are shown in Fig. 8.

In the initially steady flow, the maximum cross-correlation coefficient R_{max}, decreased with increasing separation distance Δy for all velocity components. For the longitudinal and vertical velocity components, R_{max} became negative for $\Delta y/B > 0.03$. Since the first point of the transverse profile was located at y = 0.333 m ($\Delta y/B = 0$) where y was zero at the right side wall (Fig. 2a), the points associated with negative R_{max} were in fact points on the other side of the channel centreline. The magnitudes of negative R_{max} generally increased with increasing distance from the centreline and reference point. This suggested some symmetry of velocity field about the channel centreline. Overall, the spatial variations of the maximum cross-correlation coefficient from the reference point compared well with past experimental findings in developing turbulent boundary layers [10].

During the passage of the positive surge, the cross-correlation

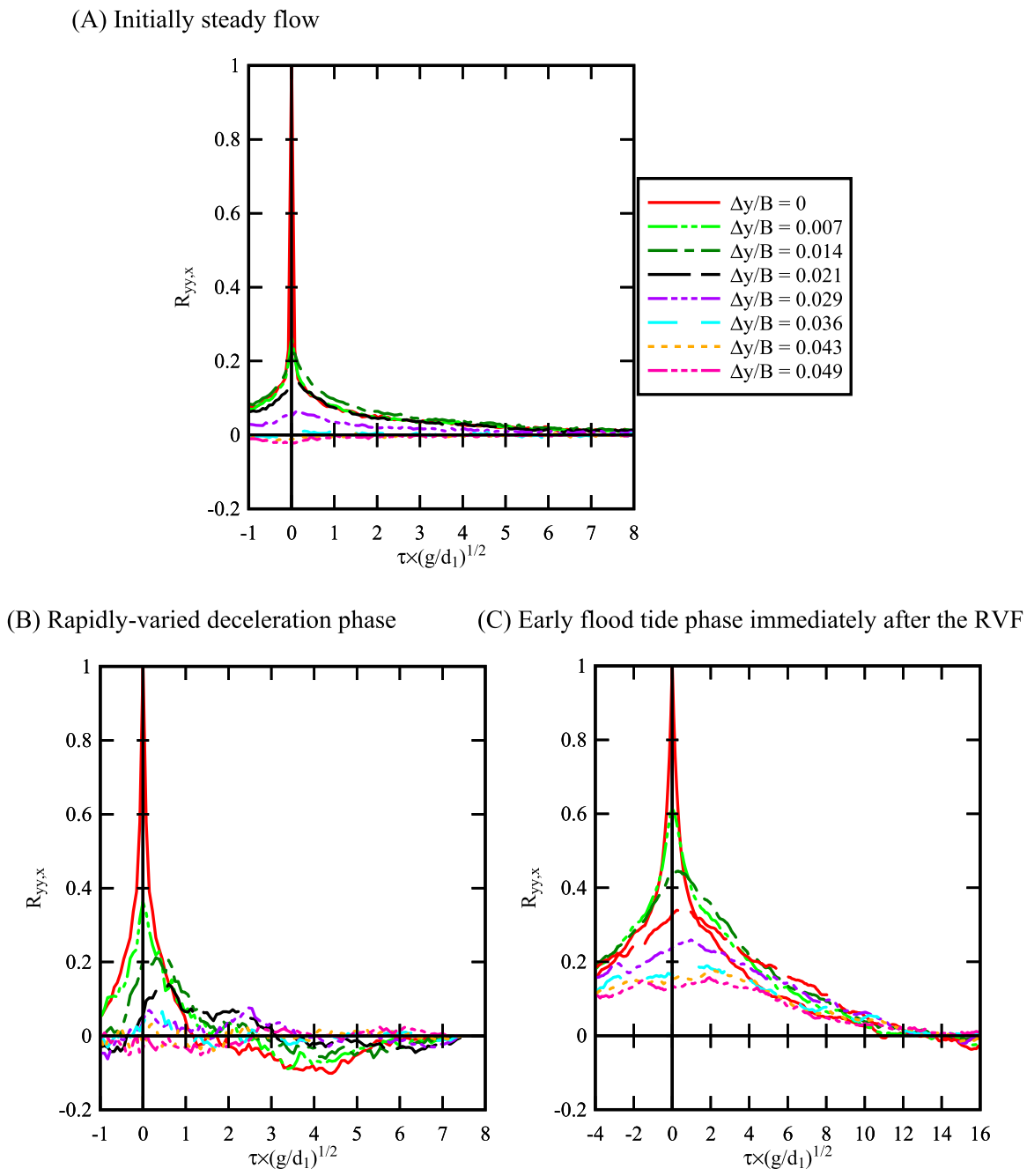

Fig. 7. Cross-correlation functions of the longitudinal velocity component at a number of transverse separations by the transverse Profiler (alone) during a positive surge - Flow conditions: Q = 0.101 m^3/s, d_1 = 0.175 m, Fr_1 = 1.47, x = 8.5 m, z/d_1 = 0.17; same legend for all graphs. (A) Initially steady flow. (B) Rapidly-varied deceleration phase. (C) Early flood tide phase immediately after the RVF.

functions showed similarities to the steady flow data, with quasi-symmetrical bell shapes and marked peaks near zero time lag. The maximum cross-correlation coefficient R_{max} at different transverse separations showed a decreasing trend with increasing time lag during the rapidly-varied deceleration flow and early flood tide phases, consistent with the findings for the steady flow phase. During the early flood tide phase, the span of cross-correlation functions at all transverse separations seemed to widen compared to the data during the earlier two phases, yielding larger area under curves (Fig. 7c). After the surge passage, immediately after the deceleration phase, the cross-correlation functions featured some unusual feature: namely two local peaks, one with positive time lags and one with negative time lags. The

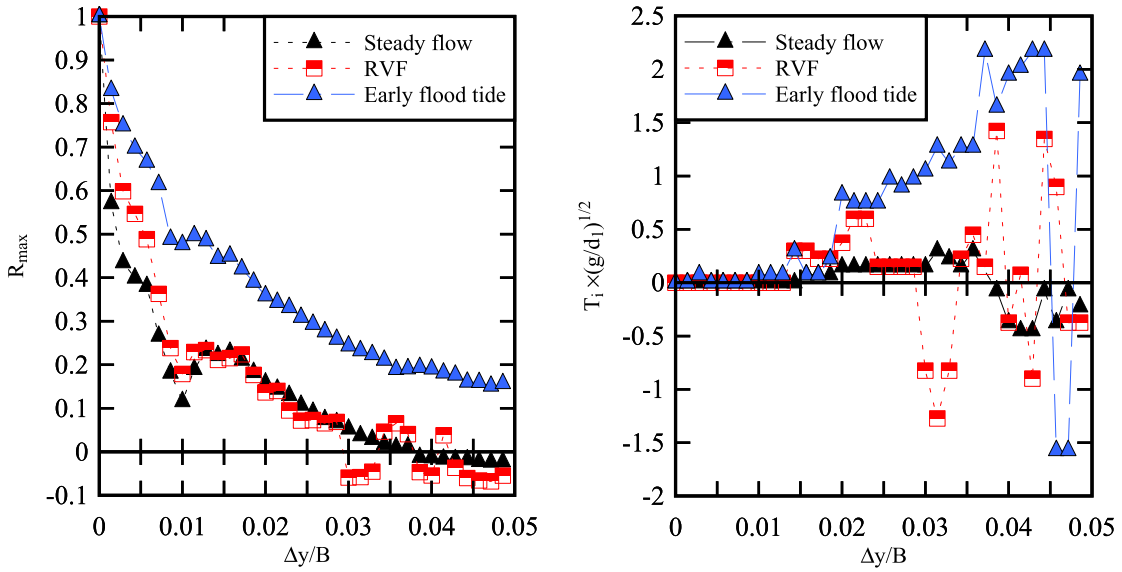

Fig. 8. Spatial variations with transverse distance of maximum cross-correlation coefficient R_{max} and optimum time lag T_i of the longitudinal velocity component during the three flow phases of a positive surge - Flow conditions: Q = 0.101 m^3/s, d_1 = 0.175 m, Fr_1 = 1.47, x = 8.5 m, z/d_1 = 0.17, transverse Profiler sampled alone.

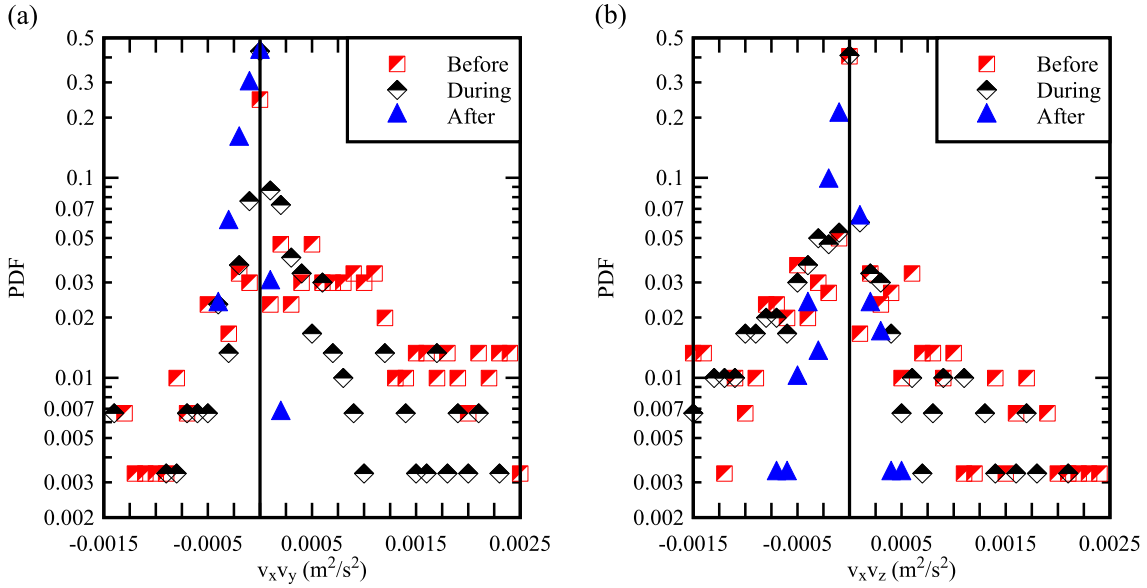

Fig. 9. Probability density functions of the tangential Reynolds stress components v_xv_y (a) and v_xv_z (b) before, during and after the positive passage for the transverse profiler - Vertical axis in logarithmic scale - Flow conditions: Q = 0.101 m^3/s, Fr_1 = 1.52, z/d_1 = 0.17, y/B = 0.50. (a, Left) Tangential stress v_xv_y. (b, Right) Tangential stress v_xv_z.

magnitudes of the negative-lagged peaks were in general less than the positive-lagged ones. The double peaks in cross-correlation functions were more remarkable for $\Delta y/B > 0.029$, suggesting that the propagation of positive was a three-dimensional phenomenon, with significant transverse recirculation occurring after the surge passage.

During the surge passage, the maximum cross-correlation coefficient decreased with increasing transverse separation from the reference point for all velocity components during all flow phases (Fig. 8, left). The early flood tide phase was associated with highest values of R_{max} for all separations. It is believed that the large amount of air bubbles entrained behind the surge led to stronger acoustic backscatter, hence the higher signal correlation. The optimum time lag T_i was zero for small separation distance from the reference point for all flow phases (Fig. 8, right). With increasing transverse separations

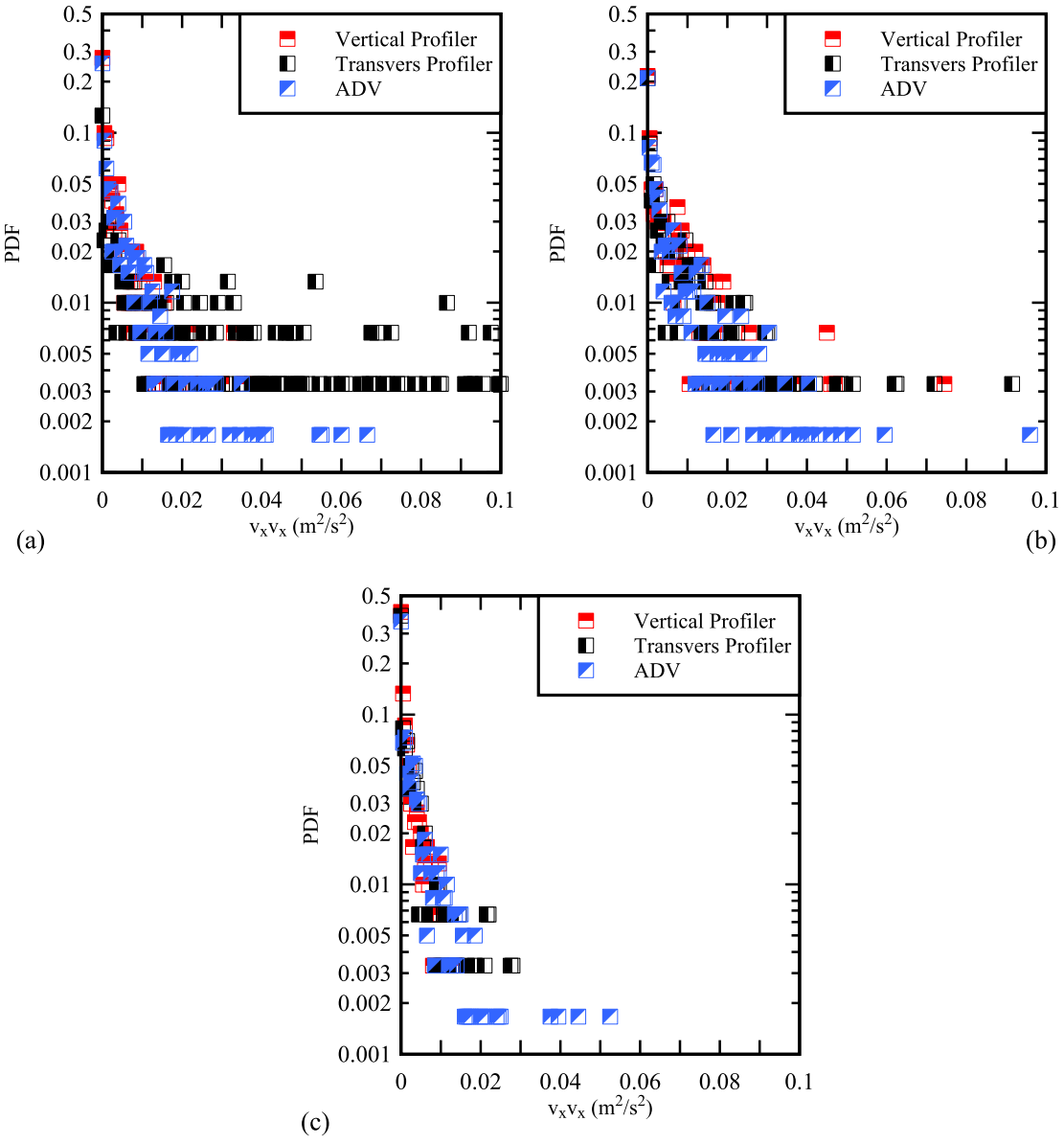

Fig. 10. Probability density functions of the instantaneous normal Reynolds stress component v_xv_x before (a), during (b) and after (c) the positive surge passage - Comparison between Profiler array and ADV data - Vertical axis in logarithmic scale - Flow conditions: Q = 0.101 m^3/s, Fr_1 = 1.52, y/B = 0.50, z/d_1 = 0.17 (Profilers) and 0.10 (ADV).

(0.01 < Δy/B < 0.03), T_i increased with increasing separations. During the rapidly-varied flow phase, the optimum time lag fluctuated between positive and negative values with a dimensionless time span between − 1.5–1.5. During the early flood tide phase, T_i kept increasing with increasing transverse separation until Δy/B > 0.045, where it became negative. The range of variation in optimum time lag during the early flood tide phase was the largest, from − 1.5–2.5 in dimensionless form.

6.3. *Turbulent time and length scales before and during a positive surge*

The integral turbulent time and length scales were calculated using Eqs. (3)–(6) for measurements with single Profiler and Profiler array, independently. The results are presented in Appendix A, including some comparison to past data [20,29]. The complete data set is detailed in Leng and Chanson [21].

Overall, the integral turbulent length scales were of an order of magnitude of 10^{-2} m to 10^{-3} m, and turbulent time scales were between 10^{-2} s and 10^{-1} s, corresponding to dimensionless length scales of $L/d_1 \sim 0.01$–0.1 and dimensionless time scales of $T \times (g/d_1)^{1/2} \sim$ 0.1–1.0. Both Profilers gave very close results, qualitatively and quantitatively, with the same data trend during the positive surge passage. The different flow phases were associated with different turbulent time and length scales. During the early flood tide phase, immediately after the rapid deceleration, both turbulent time and length scales were the

largest for all velocity components at all vertical elevations, i.e. $L_{yy,i}$ ~10^{-2} m and $T_{yy,i}$ ~10^{-1} s. The integral turbulent length scale during the early flood tide phase could be twice as large as that during the initially steady flow phase, whereas the time scale could an order of magnitude larger. The transverse turbulent length scale data, i.e. measured with the transverse Profiler, were larger in general for the transverse velocity component: $L_{yy,y}/L_{yy,x}$ ~ 2–3. The vertical turbulent length scale data, on the other hand, showed larger length scales in terms of vertical velocity component $L_{zz,z}/L_{zz,x}$ ~ 2. This could be linked to the orientation of the two sampling profiles, one of which was oriented vertically and the other one was oriented transversely. The spatial ranges of detection for the two profiles were maximised respectively along their oriented dimensions, hence the anisotropic turbulent properties. However, past experimental studies showed that open channel flows in a laboratory channel presented three-dimensional anisotropy, with turbulent length scale being larger in the longer dimension (usually the stream-wise dimension) [10,24]. Herein, the passage of the bore was associated with large increase in turbulent intensity and mixing, marked by longer time and length scales of the turbulent coherent structures underneath the flow.

The present data compared relatively well with a previous experimental data set, in terms turbulent time and length scales (Appendix A). During the early flood tide phase, the present turbulent time and length scale data were an order of magnitude higher than the findings of Simon and Chanson [29]. The difference can be attributed to the size difference of the experimental facility and instrumentation spatial resolution. The present study was performed in a large-size 0.7 m wide facility with much higher Reynolds numbers, together with simultaneous sampling for 34 transverse separations; and the results were ensemble-averaged over 25 runs. In comparison, Simon and Chanson [29] recorded 6 transverse separations with experiments repeated 5 times, for each separation: i.e., not simultaneously. Simply the present data set was associated with finer spatial resolution and stronger time correlations.

7. Discussion: turbulent Reynolds stresses

While the Reynolds stress tensor may be calculated easily in steady flows, its estimate in unsteady rapidly-varied flows relies upon ensemble-average data sets. In the present study, the instantaneous turbulent velocity fluctuation was the instantaneous deviation of the velocity data from the instantaneous ensemble-median: $v_i = V_i - \bar{V}_i$, with i = x, y, or z [5]. All the data sets, ADV and Profilers, highlighted an increase in stress magnitudes and fluctuation range for all components associated with the positive surge passage. In terms of the normal stresses, $v_x v_x$, $v_y v_y$ and $v_z v_z$, maximum ensemble-median stress magnitudes were reached shortly after the passage of the surge. This time delay was previously observed [19].

The probability density functions of ensemble-median Reynolds stress components measured by the transverse Profiler were analysed. Fig. 9 shows typical results for the tangential stress components $v_x v_y$ and $v_x v_z$ before, during and after the bore passage. For each phase, 3 s of data were analysed, in accordance to an earlier study [19]. The PDF of tangential stress components showed pseudo-Gaussian distributions before, during and after the bore arrival. The mean stresses of $v_x v_y$ were approximately zero before and during the surge passage, with a preponderance of positive stresses relative to the mean. After the surge passage, the mean stress became negative and the predominant probability was associated with negative stress values. During the surge passage, the probability of large stress magnitudes increased, while after the bore passage the stress was mainly negative. The tangential stress $v_x v_z$ showed a slightly asymmetrical single mode distribution, with a negative mode and preponderance in negative stresses throughout the surge propagation process (Fig. 9).

The probability density functions of the instantaneous Reynolds stresses were compared between the three velocimetry systems. Fig. 10 shows typical results for the normal Reynolds stress component $v_x v_x$ during different phases of a positive surge propagation. Overall, the data sets agreed in terms of PDF shape for all flow phases. For a majority of datasets (~70%), the results of the two Profilers agreed quantitatively with the ADV results. For high stress magnitudes (> 10–40 Pa), the Profiler data deviated from the ADV results, showing higher probability (~3%), compared to the ADV data (less than 1%). The results of the two Profilers showed a better agreement with the ADV data during the rapidly-varied flow, i.e. decelerating phase, and after the surge (Fig. 8a & b), as compared to the initially steady flow phase. After the surge passage, all datasets showed asymmetrical distributions of the PDF of tangential stress components. The probability of negative tangential stress was higher than that of the positive stress.

8. Conclusion

New transverse velocity profiling experiments were conducted in steady and unsteady rapidly-varied flows in a large-size facility. The measurements were performed with a transverse ADV Profiler and an array of two ADV Profilers, installed perpendicular. The results were systematically compared to ADV Vectrino + data. The turbulent time and length scales were deduced for the different flow phases of a positive surge: in the initially-steady flow before the bore, during and after the surge passage.

Ensemble-averaged velocity measurements were performed using the transverse Vectrino II Profiler alone, and sampled together with a more traditional fixed-stem Vectrino II Profiler mounted vertically. Present results demonstrated that the transverse Profiler gave satisfactory performances in a highly unsteady turbulent flow. It is acknowledged that the intrusive nature of the instrument probe and its support affected the velocity signals of downstream instruments. However the velocity signal sampled by the transverse Profiler itself was not adversely affected. The ensemble-averaged velocity and Reynolds stress characteristics measured by the transverse Profiler, alone or in an array, were very similar to results with a traditional ADV and the vertical Profiler alone, although it is acknowledged that the ADV Vectrino II Profiler instrument has intrinsic limitations at both ends of the sampling profile.

The one-dimensional integral turbulent time and length scales in the transverse or vertical directions were comparable in magnitudes, for the same flow phase, with the turbulent length scale ranging from 10^{-3} m to 10^{-2} m and turbulent time scales from 10^{-2} s and 10^{-1} s. The turbulent scale data indicated that the propagation of a positive surge was an anisotropic process, with larger length scales in the transverse component, compared to the longitudinal and vertical velocity components. The turbulent length and time scales tended to increase during and after the surge passage, in comparison to those during the initially steady flows.

Acknowledgments

The authors thank Prof Colin Rennie (University of Ottawa, Canada) and Dr Bruce MacVicar (University of Waterloo, Canada), for helpful comments. The authors acknowledge the technical assistance of Jason Van Der Gevel and Stewart Matthews (The University of Queensland). The financial support through the Australian Research Council, Australia (Grant DP120100481) is acknowledged.

Disclosure statement

The authors have no conflict of interest nor any vested interests. This is not an industry sponsored study.

Appendix A. Turbulent time and length scale results

See Tables A1 and A2.

Table A1
Turbulent time and length scales calculated from the ensemble-averaged transverse Profiler data: transverse Profiler sampled alone and sampled simultaneously with vertical Profiler (i.e. Profiler array) - Comparison with past data [29].

					Steady	flow	RVF		After	surge	Steady
Setup	Q (m^3/s)	d_1 (m)	z/d_1 ([1])	Fr_1	$L_{yy,x}/ d_1$	$T_{yy,x} \times (g/d_1)^{1/2}$	$L_{yy,x}/ d_1$	$T_{yy,x} \times (g/d_1)^{1/2}$	$L_{yy,x}/ d_1$	$T_{yy,x} \times (g/d_1)^{1/2}$	$L_{yy,y}/ d_1$
Transverse	0.101	0.176	0.17	1.55	0.005	0.041	0.006	0.024	0.012	0.223	0.012
Profiler			0.26		0.006	0.044	0.010	0.069	0.017	0.106	0.014
(alone)			0.34		0.005	0.034	0.009	0.061	0.014	0.163	0.014
Transverse	0.101	0.176	0.17	1.55	0.004	0.026	0.008	0.047	0.011	0.249	0.009
Profiler			0.26		0.003	0.047	0.006	0.031	0.012	0.243	0.008
(array)			0.40		0.002	0.017	0.006	0.038	0.009	0.159	0.006
Simon and	0.053	0.112	0.11	1.59	0.036	0.374	–	–	0.036	0.356	0.054
Chanson			0.27		0.054	0.524	–	–	0.063	0.543	0.089
(2013)			0.45		0.054	0.290	–	–	0.054	0.468	0.089
			0.63		0.045	0.103	–	–	0.063	0.477	0.080

	flow	RVF		After	surge	Steady	flow	RVF		After	surge
Setup	$T_{yy,y} \times (g/d_1)^{1/2}$	$L_{yy,y}/ d_1$	$T_{yy,y} \times (g/d_1)^{1/2}$	$L_{yy,y}/ d_1$	$T_{yy,y} \times (g/d_1)^{1/2}$	$L_{yy,z}/ d_1$	$T_{yy,z} \times (g/d_1)^{1/2}$	$L_{yy,z}/ d_1$	$T_{yy,z} \times (g/d_1)^{1/2}$	$L_{yy,z}/ d_1$	$T_{yy,z} \times (g/d_1)^{1/2}$
Transverse	0.020	0.011	0.030	0.023	0.446	0.003	0.012	0.005	0.019	0.006	0.088
Profiler	0.017	0.017	0.129	0.024	0.475	0.003	0.005	0.005	0.027	0.007	0.097
(alone)	0.017	0.017	0.124	0.023	0.447	0.004	0.013	0.005	0.026	0.006	0.057
Transverse	0.017	0.012	0.078	0.023	0.448	0.005	0.006	0.005	0.027	0.007	0.108
Profiler	0.026	0.011	0.054	0.020	0.292	0.008	0.003	0.005	0.009	0.006	0.075
(array)	0.011	0.013	0.059	0.023	0.423	0.007	0.003	0.004	0.015	0.006	0.099
Simon and	0.168	–	–	0.063	0.365	–	–	–	–	–	–
Chanson	0.187	–	–	0.089	0.459	–	–	–	–	–	–
(2013)	0.159	–	–	0.089	0.477	–	–	–	–	–	–
	0.122	–	–	0.080	0.346	–	–	–	–	–	–

Table A2
Turbulent time and length scales calculated from the ensemble-averaged vertical Profiler data: vertical Profiler sampled alone and sampled simultaneously with transverse Profiler (i.e. Profiler array).

					Steady	flow	RVF		After	surge	Steady
Setup	Q (m^3/s)	d_1 (m)	z/d_1[a]	Fr_1	$L_{zz,x}/ d_1$	$T_{zz,x} \times (g/d_1)^{1/2}$	$L_{zz,x}/ d_1$	$T_{zz,x} \times (g/d_1)^{1/2}$	$L_{zz,x}/ d_1$	$T_{zz,x} \times (g/d_1)^{1/2}$	$L_{zz,y}/ d_1$
Vertical	0.099	0.171	0.20	1.60	0.041	0.556	0.053	0.305	0.059	1.60	0.024
Profiler			0.58		0.040	0.505	0.058	0.143	0.052	1.56	0.023
(alone)[b]			0.74		0.018	0.046	0.053	0.076	0.053	1.37	0.018
Vertical	0.101	0.175	0.20	1.55	0.029	0.481	0.046	0.353	0.057	1.52	0.034
Profiler			0.28		0.023	0.269	0.028	0.105	0.063	1.56	0.034
(array)			0.43		0.017	0.276	0.034	0.224	0.057	1.53	0.028

	flow	RVF		After	surge	Steady	flow	RVF		After	surge
Setup	$T_{zz,y} \times (g/d_1)^{1/2}$	$L_{zz,y}/ d_1$	$T_{zz,y} \times (g/d_1)^{1/2}$	$L_{zz,y}/ d_1$	$T_{zz,y} \times (g/d_1)^{1/2}$	$L_{zz,z}/ d_1$	$T_{zz,z} \times (g/d_1)^{1/2}$	$L_{zz,z}/ d_1$	$T_{zz,z} \times (g/d_1)^{1/2}$	$L_{zz,z}/ d_1$	$T_{zz,z} \times (g/d_1)^{1/2}$
Vertical	0.084	0.024	0.107	0.053	1.65	0.053	0.160	0.053	0.198	0.089	1.72
Profiler	0.045	0.029	0.090	0.046	1.07	0.058	0.151	0.046	0.136	0.104	2.58
(alone)[b]	0.023	0.029	0.038	0.047	0.843	0.076	0.205	0.088	0.144	0.118	2.29
Vertical	0.113	0.034	0.195	0.063	2.07	0.046	0.263	0.063	0.435	0.098	2.45
Profiler	0.067	0.040	0.217	0.051	1.04	0.045	0.373	0.045	0.246	0.102	1.95
(array)	0.037	0.023	0.075	0.051	1.27	0.034	0.284	0.040	0.172	0.080	1.72

Notes:
[a] : $(z/d_1)_{max}$ for vertical Profiler.
[b] : experiments from Leng and Chanson [20].

References

[1] M. Bahreinimotlagh, K. Kawanisi, M.M. Danial, M.B. Al Sawaf, J. Kagami, Application of shallow-water acoustic tomography to measure flow direction and river discharge, Flow. Meas. Instrum. 51 (2016) 30–39.

[2] J. Becker, VTMT (Version 1.1) [Computer software], Federal Waterways Engineering and Research Institute (BAW), Karlsruhe, Germany, 2014〈http://sdrv.ms/12eHgvw/〉 (Accessed 19 November 2014).

[3] H. Chanson, "Acoustic Doppler Velocimetry (ADV) in the Field and in Laboratory: Practical Experiences", in: Proceedings of the International Meeting on Measurements and Hydraulics of Sewers IMMHS'08, Summer School GEMCEA/LCPC, 19–21 Aug. 2008, Bouguenais, FrédériqueLarrarte and Hubert Chanson Editors., Hydraulic Model Report No. CH70/08, Div. of Civil Engineering, The University of Queensland, Brisbane, Australia, Dec., 2008, pp. 49–66.

[4] H. Chanson, Tidal Bores, Aegir, Eagre, Mascaret, Pororoca: Theory and Observations, World Scientific, Singapore, 2011, p. 220.

[5] H. Chanson, N.J. Docherty, Turbulent velocity measurements in open channel bores, Eur. J. Mech. B/Fluids 32 (2012) 52–58, https://doi.org/10.1016/j.euromechflu.2011.10.001.

[6] R.G.A. Craig, C. Loadman, B. Clement, P.J. Ruesello, E. Siegel, "Characterization and Testing of a new Bistatic Profiling Acoustic Doppler Velocimeter: The Vectrino-II," IEEE/OES/CWTM, in: Proceedings of the 10th Working Conference on Current, Waves and Turbulence Measurement (CWTM), Monterey, Canada, 20–23 March, 2011, pp. 246–252 〈http://dx.doi.org/10.1109/CWTM.2011.5759559〉.

[7] J.A. Cunge, Rapidly varying flow in power and pumping canals, in: K. Mahmood, V. Yevdjevich (Eds.), Unsteady Flow in Open Channels, 2 WRP Publ, Fort Collins, USA, 1975, pp. 539–586.

[8] S. Dilling, B.J. Macvicar, Cleaning high-frequency velocity profile data with auto-regressive moving average (ARMA) models, Flow. Meas. Instrum. 54 (2017) 68–81.

[9] A.J. Favre, J.J. Gaviglio, R. Dumas, Space-time double correlations and spectra in a turbulent boundary layer, J. Fluid Mech. 2 (1957) 313–342.

[10] A.J. Favre, Review on space-time correlations in turbulent fluids, J. Appl. Mech. ASME 32 (2) (1965) 241–257.

[11] H.M. Fritz, W.H. Hager, H.E. Minor, Near field characteristics of landslide generated impulse waves, J. Waterw. Port Coast. Ocean Eng. ASCE 130 (6) (2004) 287–302, https://doi.org/10.1061/(ASCE)0733-950X(2004)130:6(287).

[12] A. Hauet, J. Le Coz, G. Dramais, C. Carre, D. Legras, G. Pierrefeu, C. Godayer, Innovating methods for continuous river discharge monitoring: horizontal fixed Doppler profiler (H-aDcp) and image analysis (LSPIV), La Houille Blanc.-Rev. Int. De. l'Eau 3 (2009) 123–131, https://doi.org/10.1051/lhb/2009036.

[13] F.M. Henderson, Open Channel Flow, MacMillan Company, New York, USA, 1966.

[14] H.G. Hornung, C. Willert, S. Turner, The flow field downstream of a hydraulic jump, J. Fluid Mech. 287 (1995) 299–316.

[15] C. Koch, H. Chanson, Turbulence measurements in positive surges and bores, J. Hydraul. Res. IAHR 47 (1) (2009) 29–40, https://doi.org/10.3826/jhr.2009.2954.

[16] J. Le Coz, G. Pierrefeu, A. Paquier, Evaluation of river discharges monitored by a fixed side-looking Doppler profiler (Paper W00D09), Water Resour. Res. 44 (2008) 13, https://doi.org/10.1029/2008WR006967.

[17] X. Leng, A Study of Turbulence: the Unsteady Propagation of Bores and Surges (Ph.D. Thesis), The University of Queensland, School of Civil Engineering, Brisbane, Australia, 2018.

[18] X. Leng, H. Chanson, Breaking bore: physical observations of roller characteristics, Mech. Res. Commun. 65 (2015) 24–29, https://doi.org/10.1016/j.mechrescom.2015.02.008.

[19] X. Leng, H. Chanson, Coupling between free-surface fluctuations, velocity fluctuations and turbulent Reynolds stresses during the upstream propagation of positive surges, bores and compression waves (digital appendix), Environ. Fluid Mech. 16 (4) (2016) 695–719, https://doi.org/10.1007/s10652-015-9438-8.

[20] X. Leng, H. Chanson, Unsteady velocity profiling in bores and positive surges, Flow. Meas. Instrum. 54 (2017) 136–145, https://doi.org/10.1016/j.flowmeasinst.2017.01.004.

[21] X. Leng, H. Chanson, Simultaneous velocity profiling in unsteady turbulent flows using an array of two vectrino profilers, Hydraulic Model Report No. CH106/17, School of Civil Engineering, The University of Queensland, Brisbane, Australia, 2018, p. 134.

[22] B. Macvicar, S. Dilling, J. Lacey, K. Hipel, "A Quality Analysis of the Vectrino II Instrument using a New Open-source MATLAB Toolbox and 2D ARMA Models to Detect and Replace Spikes," in: Proceedings of the 7th International Conference on Fluvial Hydraulics (River Flow), Lausanne, Switzerland, 3–5 Sept., 2014, pp. 1951–1959.

[23] D.J. Miller, Giant waves in Lituya Bay, Alaska, Geological Survey Professional Paper 354-C, U.S. Government Printing Office, Washington D.C., 1960, pp. 51–86.

[24] H. Nakagawa, I. Nezu, Structure of Space-Time Correlations of Bursting Phenomena in an Open-Channel Flow, J. Fluid Mech. 104 (1981) 1–43.

[25] Nortek, "Vectrino Profiler: User Guide." Nortek Scientific Acoustic Development Group Inc., User Manual, 2012.

[26] J. Ponsy, M. Carbonnell, Etude Photogrammétrique d'Intumescences dans le canal de l'Usine d'Oraison (Basses-Alpes). ('Photogrammetric study of positive surges in the Oraison Powerplant canal.') *Jl Soc*, Fr. De. Photo. 22 (1966) 18–28 (in French).

[27] B. Simon, Effects of Tidal Bores on Turbulent Mixing: a Numerical and Physical Study in Positive Surges (Ph.D. Thesis), School of Civil Engineering, The University of Queensland, Brisbane, Australia, 2014, p. 259, https://doi.org/10.14264/uql.2014.19.

[28] H. Tanaka, N.X. Tinh, N.X. Dao, "Field Measurement and Numerical Studies on the Tsunami Propagation into Upstream Rivers," in: Proceedings of the 34th IAHR World Congress, Brisbane, Australia, 26 June-1 July, Engineers Australia Publication, Eric Valentine, ColinApelt, James Ball, Hubert Chanson, Ron Cox, Rob Ettema, George Kuczera, Martin Lambert, Bruce Melville and Jane Sargison Editors, 2011, pp. 1317–1324.

[29] B. Simon, H. Chanson, Turbulence measurements in tidal bore-like positive surges over a rough bed, Hydraulic Model Report No. CH90/12, School of Civil Engineering, The University of Queensland, Brisbane, Australia, 2013, p. 176.

[30] R.E. Thomas, L. Schindfessel, S.J. McLelland, S. Creelle, T. De Mulder, Bias in mean velocities and noise in variances and covariances measured using a multistatic acoustic profiler: the Nortek Vectrino Profiler (Paper 075302), Meas. Sci. Technol. 28 (2017) 25, https://doi.org/10.1088/1361-6501/aa727.

[31] L. Zedel, A. Hay, "Turbulence Measurements in a Jet: Comparing the Vectrino and Vectrino II," IEEE/OES/CWTM, in: Proceedings of the 10th Working Conference on Current, Waves and Turbulence Measurements (CWTM), Monterey, Canada, 20–23 March, 2011, pp. 173–178 〈http://dx.doi.org/10.1109/CWTM.2011.5759547〉.

[32] H. Chanson, Atmospheric Noise of a Breaking Tidal Bore, J. Acoust. Soc. Am. 139 (1) (2016) 12–20, https://doi.org/10.1121/1.4939113.

Xianqian Leng is a postdoctoral research fellow at the University of Queensland. Her research interests include experimental investigations of unsteady rapidly-varied open channel flows, computational fluid dynamics (CFD) modelling of bores and positive surges, and field investigations of tidal bores. She authored 41 peer-reviewed papers, including 18 international scientific journal articles.

Hubert Chanson is a Professor in Civil Engineering, Hydraulic Engineering and Environmental Fluid Mechanics at the University of Queensland, Australia. His research interests include design of hydraulic structures, experimental investigations of two-phase flows, applied hydrodynamics, hydraulic engineering, water quality modelling, environmental fluid mechanics, estuarine processes and natural resources. His publication record includes over 850 international refereed papers and several books, and his work was cited more than 4350 times (WoS) to 15,500 times (Google Scholar) since 1990. In 2018, his h-index was 35 (WoS), 38 (Scopus) and 62 (Google Scholar).